International Journal of Bifurcation and Chaos, Vol. 33, No. 9 (2023) 2330022 (12 pages)

DOI: 10.1142/S0218127423300227

Basin Entropy and Wada Property of Magnetic Field Line Escape in Toroidal Plasmas with Reversed Shear

P. Haerter*, L. C. de Souza, A. C. Mathias and R. L. Viana
Department of Physics, Federal University Paraná,
81531-990 Curitiba, Paraná, Brazil
**haerter@fisica.ufpr.br*

I. L. Caldas
Institute of Physics, University of São Paulo,
05315-970 São Paulo, São Paulo, Brazil

Received February 24, 2023; Revised June 5, 2023

The structure of magnetic field lines in toroidal fusion plasmas, as in tokamaks and stellarators, represents the lowest-order description of the plasma particle behavior, up to finite Larmor and drift effects. Tokamaks with reversed magnetic shear typically present internal transport barriers that help to improve confinement through a partial or total reduction of the particle transport across magnetic surfaces. In this work, we investigate numerically particle escape in tokamaks with reversed shear in order to identify fractal structures affecting transport. These structures are quantitatively evaluated using two basic measures: the basin entropy and the Wada property.

Keywords: Tokamak; reversed shear; escape basin; basin entropy; Wada property; fractal basin boundary; transport barrier; chaotic transport.

1. Introduction

Nonintegrable Hamiltonian systems appear in various physical applications involving fluids and plasmas, like passive advection in plane incompressible flows, vortex motion in two dimensions, and magnetic field lines in fusion plasmas, among other examples [Lichtenberg & Lieberman, 2013]. One of the well-known features of nonintegrable systems is the existence of chaotic orbits, for which there is an extreme sensibility to the initial conditions, combined with aperiodic behavior [Ott, 2002]. When a chaotic orbit occupies a significant region of the available phase space, it is important to understand qualitatively and quantitatively the chaotic transport over such a region [Wiggins, 2013].

Plasma physics is one of the scientific fields where chaotic transport encounters a large number of applications, especially in the study of magnetic confinement plasmas [Hazeltine & Meiss, 2003]. Toroidal plasma devices, like Tokamaks and Stellarators, display many situations where nonsymmetrical and/or time-dependent perturbation leads to chaotic motion, resulting in chaotic transport, also known as anomalous transport in plasma literature [Balescu, 1988]. Hence the understanding of the physical factors influencing chaotic transport is a key to develop forms of control for a number of undesirable effects, like loss of confinement.

It has been recently argued that, in toroidal plasmas with reversed shear, internal transport barriers can be formed, so reducing the levels of chaotic transport, resulting in a better quality of plasma confinement [Viana *et al.*, 2021]. Such transport barriers are internal and partial, in the sense that

they allow some degree of transmission [Wolf, 2002]. Simple dynamical models, like the so-called standard nontwist map, are able to describe the formation of internal transport barriers [del Castillo-Negrete & Morrison, 1993]. In the context of plasma physics, a related model was proposed by Balescu, in the form of an area-preserving two-dimensional map (revtokamap), which displays the essential features present in tokamak plasmas with reversed magnetic shear [Balescu, 1998].

The revtokamap describes the dynamics of magnetic field lines in a suitable Poincaré surface of section. Since charged plasma particles tend to execute gyration along the field lines, if we neglect finite gyroradius and drift effects, the resulting map can be regarded as a lowest-order description of the particle behavior, especially chaotic transport [Balescu *et al.*, 1998]. Internal transport barriers affect primarily the escape of particles, and one way to investigate these effects is to make a dynamical characterization of the field line escape through the tokamak wall [Mathias *et al.*, 2017].

In the present paper, we investigate the escape of map trajectories, i.e. magnetic field lines, through the tokamak wall (that can be replaced by any boundary surface, like a divertor plate, for example), by revealing the topological and metrical properties of the corresponding escape basins [Mathias *et al.*, 2022]. Due to the nonattracting invariant set (chaotic saddle) underlying the dynamics in the chaotic region, we can characterize fractal properties of the escape basins and their boundaries [Aguirre *et al.*, 2009].

We will undergo such a quantitative study by evaluating the escape basin entropy and the basin boundary entropy, which are also useful to quantify final-state uncertainty in this system [Daza *et al.*, 2016]. Finally, in the case of three or more exits, we also characterize the so-called Wada property, which is an extreme form of final-state uncertainty [Daza *et al.*, 2015]. These measures offer valuable insights into the complexity and mixing properties of the RevTokamap, enabling us to gain a better understanding of its underlying dynamics and transport phenomena within the tokamak with the presence of reversed shear.

The rest of this paper is organized as follows: Sec. 2 will describe the magnetic field line nontwist map to be used in the numerical simulations reported in this work. In Sec. 3, we will describe the formation of internal transport barriers in the map model. Section 4 contains a qualitative discussion of the escape basins and why fractal structures appear in this context. The basin entropy and basin boundary entropy are described in Sec. 5, whereas Sec. 6 discusses the Wada property and its characterization. The last section contains our conclusions.

2. Magnetic Field Line Nontwist Map

Using an ideal magnetohydrodynamical (MHD) description for the plasma magnetically confined in a tokamak, in the equilibrium situation it turns out that the expansion caused by kinetic pressure p must be counterbalanced by a force resulting from a magnetic field $\mathbf{B}$. The equilibrium condition thus reads [Bittencourt, 2004]

$$\nabla p = \mathbf{J} \times \mathbf{B}, \tag{1}$$

where $\mathbf{J}$ is the current density of the plasma. From dotting this expression with $\mathbf{B}$, it follows immediately that

$$\mathbf{B} \cdot \nabla p = 0, \tag{2}$$

in such a way that, in an equilibrium configuration, the magnetic field lines must lie on constant pressure surfaces, also called flux surfaces or magnetic surfaces [Hazeltine & Meiss, 2003]. In a tokamak, these surfaces have a toroidal shape, with a common axis we call the magnetic axis.

It is convenient to use a special coordinate system to describe the magnetic field lines in a tokamak plasma. In Fig. 1, we represent schematically this system, also called *natural coordinates* (ψ, θ, ζ). The poloidal (θ) and toroidal (ζ) angles correspond, respectively, to the minor and major circuits along the torus. The coordinate ψ, on its

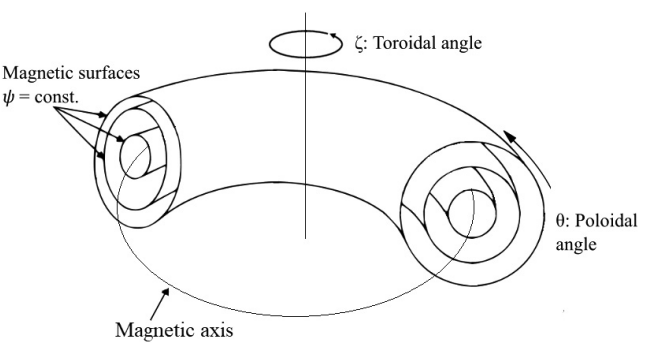

Fig. 1. Schematic figure of a tokamak showing the definition of the natural coordinates.

hand, is a radial-like coordinate that can be thought as a label for the magnetic surfaces.

One simple example of a radial-like coordinate [Hazeltine & Meiss, 2003] ψ is the volume enclosed by a given magnetic surface. Accordingly, we will choose $\psi = 0$ as the position of the magnetic axis (a degenerate magnetic surface of zero volume) (see Fig. 1). However, a more useful choice is ψ being interpreted as the toroidal flux, i.e. the magnetic flux enclosed by a magnetic surface. We can normalize this toroidal flux by dividing it by the factor $B_0 a^2$, where B_0 is the toroidal magnetic field at $\psi = 0$ and a is a characteristic plasma radius. If the magnetic surfaces have a circular cross-section, the parameter a can be interpreted as the radius of the plasma boundary.

The differential equations for the magnetic field lines are, in this coordinate system,

$$\frac{d\theta}{d\zeta} = \frac{\partial \alpha}{\partial \psi}, \quad \frac{d\psi}{d\zeta} = -\frac{\partial \alpha}{\partial \theta}, \tag{3}$$

where $\alpha(\psi, \theta)$ is the poloidal flux, i.e. the magnetic flux through a ribbon-like surface bounded from below by the magnetic axis and from above by a magnetic surface [Hazeltine & Meiss, 2003]. Although the configuration here described is strictly time-independent, we can define a timelike variable as the normalized toroidal angle $t = \zeta/(2\pi)$, in such a way that the dynamics have to be taken in a Lagrangian sense: one follows the consecutive turns of a given field line over the toroidal direction.

In the context of this description, we can define a coordinate $q = \theta/(2\pi)$ and a canonically conjugated momentum $p = \psi/(B_0 a^2)$, in such a way that the field line equations (3) can be cast into a Hamiltonian form [Lichtenberg & Lieberman, 2013]

$$\frac{dq}{dt} = \frac{\partial H}{\partial p}, \quad \frac{dp}{dt} = -\frac{\partial H}{\partial q}, \tag{4}$$

where we define a field line Hamiltonian $H(p, q, t) = \alpha(\psi, \theta, \zeta)/(B_0 a^2)$ which can be, in general, "time"-dependent. Since there is only one degree of freedom involved, if the Hamiltonian is "time"-independent, it turns out that H is a constant of motion, hence the system is integrable. On the other hand, if H depends on t, the magnetic field line system becomes nonintegrable and complex dynamics are possible, including a kind of field line chaos (taken in the above mentioned Lagrangian sense).

Apart from the different physical meanings of the timelike variable, the trajectories generated by Eq. (4) can be numerically obtained, once the Hamiltonian is known for a given situation. Since t is defined modulo 2π, we can make a Poincaré surface of section sampling variables ψ and θ at times $t = n = 0, 1, 2, \ldots$, where n is an integer, and define the corresponding discrete variables obeying a Poincaré map of a general form

$$\psi_{n+1} = f(\psi_n, \theta_n), \quad \theta_{n+1} = g(\psi_n, \theta_n), \tag{5}$$

where f and g are functions that depend on the Hamiltonian and its partial derivatives. The condition $\nabla \cdot \mathbf{B} = 0$ implies magnetic flux conservation in the context of MHD equations. From the dynamical point of view, this implies that the map (5) is area-preserving, i.e. its Jacobian determinant must be equal to unity for all times,

$$\begin{vmatrix} \dfrac{\partial f}{\partial \psi_n} & \dfrac{\partial f}{\partial \theta_n} \\ \dfrac{\partial g}{\partial \psi_n} & \dfrac{\partial g}{\partial \theta_n} \end{vmatrix} = 1. \tag{6}$$

Starting from the case of an equilibrium configuration, since field lines are bound to lie over magnetic surfaces, for which Ψ is a constant, there results that the equilibrium map is

$$\psi_{n+1} = \psi_n, \quad \theta_{n+1} = \theta_n + W(\psi_{n+1}), \tag{7}$$

where $W(\psi)$ is the winding number for the corresponding magnetic surface, measuring the advance of the poloidal angle after a complete toroidal turn of the field line. Here W is expressed in terms of ψ_{n+1} rather than ψ_n, since we interpret the map (7) as a canonical transformation from the old variables (ψ_n, θ_n) to new variables $(\psi_{n+1}, \theta_{n+1})$. Using a generating function of the second kind $F_2(\psi_{n+1}, \theta_n)$ there follows that the functions f and g in the general mapping (5) must involve the pair (ψ_{n+1}, θ_n) [Lichtenberg & Lieberman, 2013].

Considering that the plasma radius corresponds to $\psi = 1$, if the winding number profile W is a monotonic function of ψ inside the interval $0 \leq \psi \leq 1$, we see that (7) is a simple twist map, whose properties have been extensively studied. However, when studying the formation and properties of internal transport barriers, a nonmonotonic winding number profile is a suitable alternative, presenting at least one value of ψ for which the derivative of W vanishes. This is the case, for example, of the profile introduced by Balescu

$$W(\psi) = w[1 - a(c\psi - 1)^2], \tag{8}$$

where w, a and c are parameters whose values can be adapted so as to replicate profiles of interest in tokamaks with reversed shear configurations. In the following, we choose their values so that $W_0 = 0.333$ and $W_1 = 0.1667$ are the winding number value at the magnetic axis ($\psi = 0$) and plasma boundary ($\psi = 1$), respectively. Moreover, the profile has a maximum $w = 0.6667$ at a point $\psi_M = 0.0000$. Since the profile is nonmonotonic, the corresponding map (7) is nontwist, with some properties distinct from twist maps, as has been recently studied in the dynamical systems literature [Viana *et al.*, 2021; Wolf, 2002; del Castillo-Negrete & Morrison, 1993].

Now we consider the effect of a "time"-dependent magnetic perturbation produced by magnetic fields depending on all variables (ψ, θ, ζ). This perturbation can be due to external nonsymmetric magnetic fields or internal magnetic instabilities. The exact form of this perturbation term depends on the specific problem to be taken into account. However, Balescu has proposed a paradigm map, called Revtokamap, for which the perturbation has a standard form:

$$\psi_{n+1} = \psi_n - \frac{K}{2\pi}\frac{\psi_{n+1}}{1+\psi_{n+1}}\sin(2\pi\theta_n), \tag{9}$$

$$\theta_{n+1} = \theta_n + W(\psi_{n+1}) - \frac{K}{(2\pi)^2}\frac{\psi_{n+1}}{(1+\psi_{n+1})^2}\cos(2\pi\theta_n), \tag{10}$$

where $K > 0$ represents the intensity of the perturbation, such that in the case $K = 0$ we return to the nontwist map (7).

The special form of perturbation in the revtokamap (9) and (10) satisfies two important constraints from the physical point of view: (i) the radial variable ψ is always non-negative for any

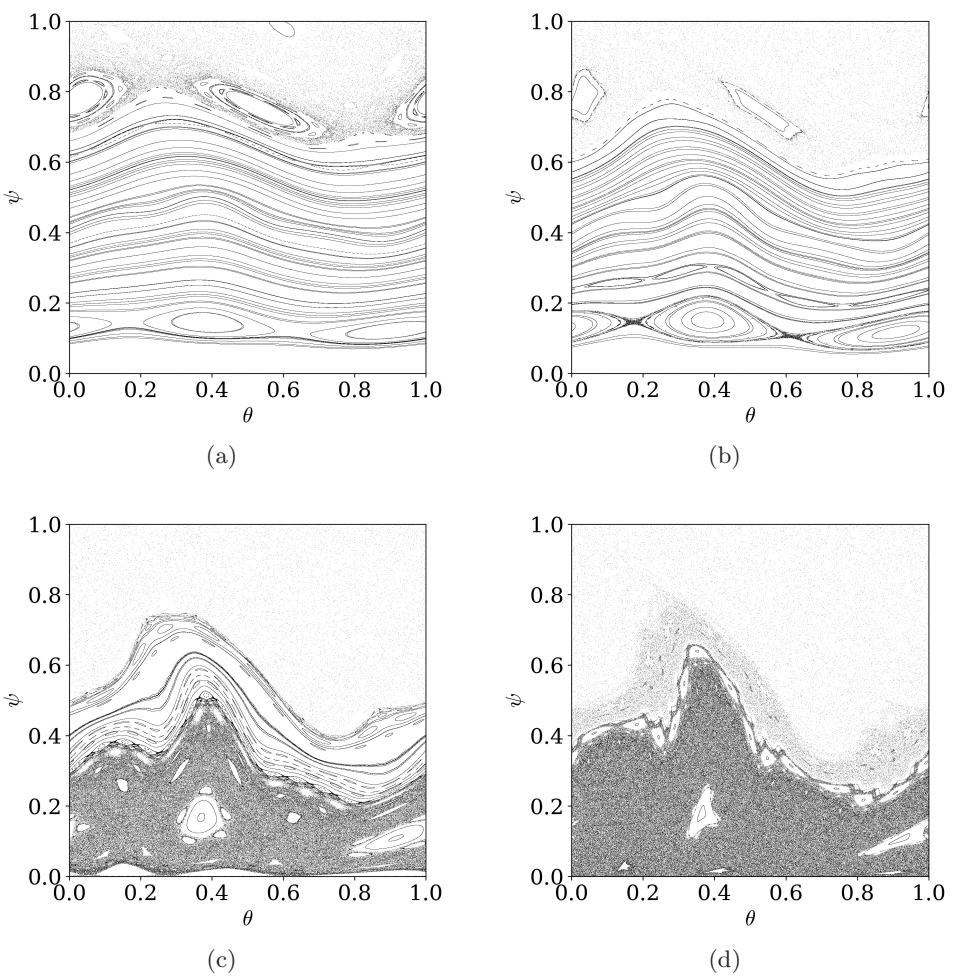

Fig. 2. Phase portraits of the Revtokamap for K = (a) 2.0, (b) 3.0, (c) 5.1 and (d) 6.3. The plots illustrate the loss of periodicity in the phase space as K increases, highlighting the presence of a transport barrier that prevents field lines from the inner part of the tokamak from escaping.

value of the parameters; (ii) the magnetic axis $\psi = 0$ is invariant under the map, i.e. if $\psi_0 = 0$ then $\psi_n = 0$ for all times. Since ψ_{n+1} enters quadratically in the map equations, we can solve them for it, retaining only the positive root, as follows

$$\psi_{n+1} = \frac{1}{2}\{P(\psi_n, \theta_n) + \sqrt{[P(\psi_n, \theta_n)]^2 + 4\psi_n}\}, \tag{11}$$

where

$$P(\psi_n, \theta_n) = \psi_n - 1 - \frac{K}{2\pi}\sin(2\pi\theta_n). \tag{12}$$

A detailed analysis of the basic dynamical properties of the revtokamap, including the families of fixed points as well as bifurcation phenomena, can be followed in [Balescu *et al.*, 1998]. In this work, we will rather focus on the chaotic field line escape. The basic idea is that, in the zeroth approximation, charged particles tend to follow the magnetic field lines, up to drift effects caused by finite Larmor radius, curvature, grad-B drifts, and so on. In this sense, the diffusion of chaotic magnetic field lines furnishes important information on the anomalous diffusion of particles.

In the following, we proceed to a numerical investigation of the dynamics displayed by the revtokamap. Keeping the parameters of the winding number profile fixed, the only tunable parameter remaining is the perturbation strength kept between $0 \leq K \leq 2\pi$. Varying its value we obtain different phase portraits, as illustrated by Figs. 2(a)–2(d).

3. Internal Transport Barrier

The *RevTokamap* introduced by Balescu has many interesting physical properties and it is suitable to describe magnetic field line structure in a tokamak with reversed shear profiles. However, it is complex enough to direct an approach to the formation and destruction of the magnetic islands and the consequent formation of an internal transport barrier. On the other hand, Del-Castillo Negrete and Morrison have previously introduced the so-called standard nontwist map which, in our variables, read [del Castillo-Negrete & Morrison, 1993]

$$y_{n+1} = y_n - \beta\sin(2\pi x_n), \tag{13}$$

$$x_{n+1} = x_n + \sigma(1 - y_{n+1}^2), \tag{14}$$

where $0 < \sigma < 1$ and $\beta > 0$ are system parameters, and $-1/2 \leq x \leq 1/2$, whereas $-\infty < y < \infty$. The latter condition is only of mathematical nature and thus cannot be realized by magnetic field lines in a tokamak, which were obviously bounded by physical limitations.

The map above displays essentially the same nontwist behavior as the Revtokamap, but with less analytical effort. Hence, in order to understand the formation of internal transport barriers we will resort to this simpler system, for which the nonmonotonic winding number is given by

$$W(y) = \sigma(1 - y^2), \tag{15}$$

and thus have a single maximum at $\psi_M = 0$. The latter defines a shearless curve since the shear therein vanishes. The quadratic form of $W(\psi)$ around $\psi_M = 0$ leads to two invariant curves at $\psi = \pm\psi_0$ with the same winding number $\sigma(1-\psi_M^2)$ on both sides of the shearless curve. As the perturbation parameter vanishes ($\beta = 0$), it turns out that two periodic island chains appear at the two invariant curve locations, and the former shearless curve becomes a shearless invariant curve separating these two periodic island chains.

In this discussion of the standard nontwist map, let us consider a fixed value of $\beta = 0.6$ and a tunable parameter σ. If $\sigma = 0.364$ the corresponding phase portrait exhibits two island chains with three islands each, with winding number $W = 0.333$, such that in the $\beta = 0$ case the invariant curves are located at $\psi = \pm 0.42$ [Fig. 3(a)]. Between these island chains, there is a shearless invariant curve, and there is no transport across it. In order to illustrate this point, in Fig. 3(a) we distinguish, using different colors, map orbits going to $\psi = \pm\infty$. These chaotic orbits are clearly separated by the twin island chains containing the shearless curve.

As the parameter σ increases its value, the island chains with the same winding number on both sides of the shearless curve approach each other. A distinctive characteristic of nontwist maps is that the island chains do not overlap according to the Chirikov condition, but instead their corresponding unstable and stable invariant manifolds suffer reconnection. After such a reconnection occurs, there appear new invariant curves (or meanders), which are distinct from KAM-type invariant curves since the latter must be graphed over the variable θ, while meanders are not [Szezech Jr *et al.*, 2012].

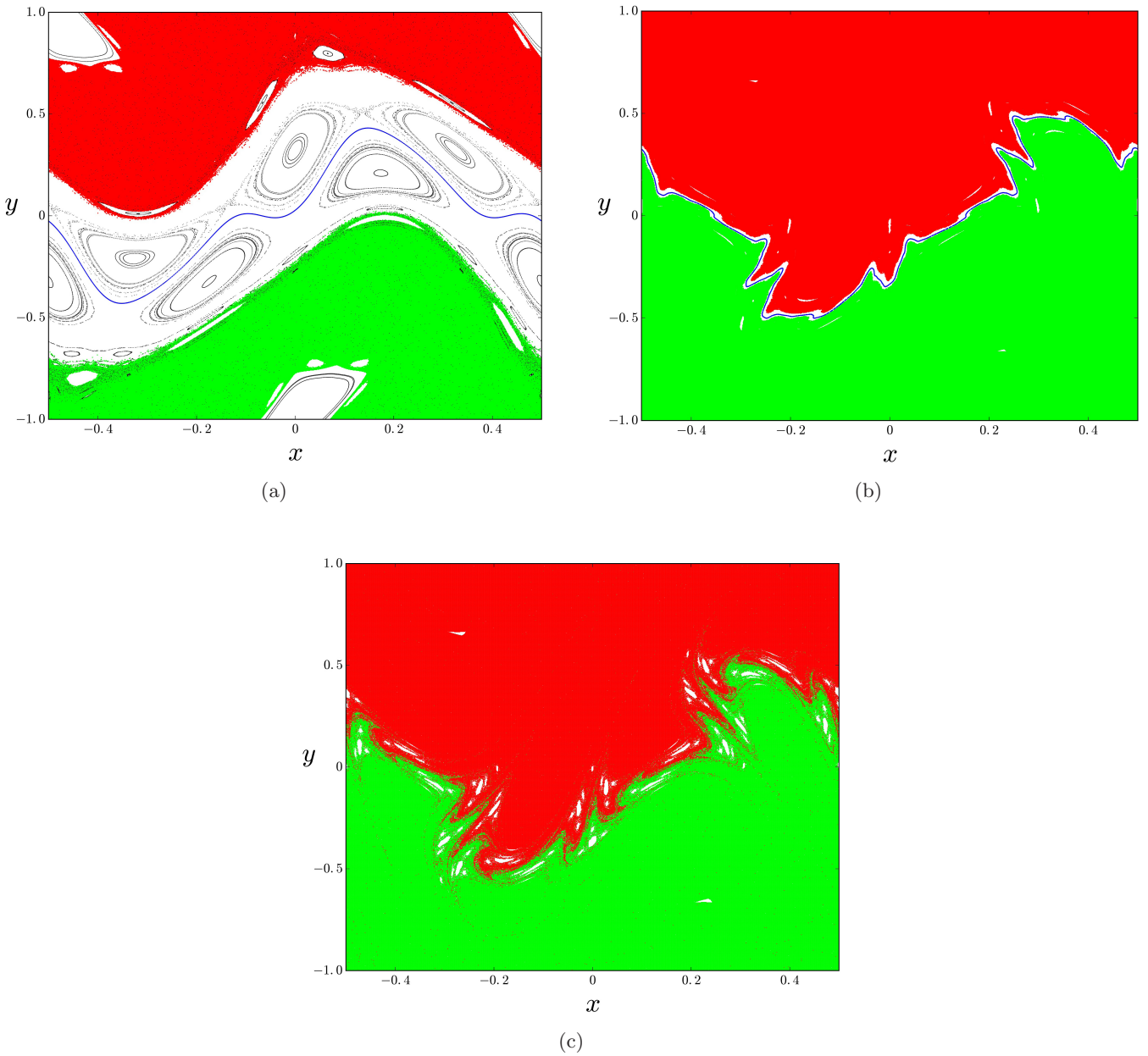

Fig. 3. Phase portraits of the standard nontwist map for $\beta = 0.6$ and $\alpha =$ (a) 0.364, (b) 0.8 and (c) 0.807. Showing the presence of the transport barrier that can be related to the revtokamap.

Increasing further the value of σ, in the phase plane region between the chains, the remaining periodic orbits eventually coalesce and disappear, leaving only meanders and the shearless torus [Fig. 3(b)]. This is still an example of a robust transport barrier since those chaotic orbits diverging to $\psi = \pm\infty$ do not mix due to the presence of a shearless curve. Another increase in a causes the breakup of the shearless curve and the mixing of these diverging chaotic orbits [Fig. 3(c)].

However, the chaotic transport therein is not uniform: we see in Fig. 3(c) that each chaotic orbit spends a long time near a remnant pair of period-11 island chains. This is a classical manifestation of stickiness, and after some (possibly long) time a chaotic orbit leaves the neighborhood of these islands, after escaping through the holes of a cantorus. The stickiness phenomenon in this region occurs to a topological reordering of the invariant stable and unstable manifolds of periodic orbits embedded in the chaotic region that follows the breakup of the last shearless curve, and thus can be regarded as a partial, or internal transport barrier [Szezech Jr *et al.*, 2012].

Although the above described scenario was described by the standard nontwist mapping, it can also be observed in other nontwist systems like the revtokamap. In a contrast with what has been just described for the standard nontwist map, in the revtokamap, we note the presence of a large chaotic region in the upper part of the phase portraits displayed by Figs. 2(a)–2(d). This difference is due to the fact that the upper twin island chain related to the broken shearless curve, in the revtokamap case, is located at large values of ψ, hence out of the physical range $0 \leq \psi \leq 1$ and thus cannot be observed. As a consequence, this outer chaotic region is bounded only below by a KAM barrier represented by invariant curves.

Therefore in the revtokamap, the chaotic transport is unidirectional, meaning that magnetic field lines can diffuse from the plasma region (low ψ) to the plasma edge (ψ near the unity). Indeed, in Figs. 2(a) and 2(b) we can observe chaotic orbits on both sides of the phase space region containing meanders and the shearless curve, forming a robust transport barrier. An increase in the value of the perturbation strength K causes this barrier to break up, forming a string of small island chains due to reconnection phenomena among invariant manifolds [Fig. 2(c)]. A further increase in K leaves this internal partial transport barrier with a single chain of 15 islands [Fig. 2(d)].

It is worth mentioning that the lower-ψ region corresponds to the plasma core, whereas larger ψ is related to the edge plasma region. The presence of an internal transport barrier produces an insulation of the plasma core, diminishing chaotic field line (and particle) transport and potentially improving the quality of plasma confinement. But, since at $\psi = 1$ we have a physical barrier (the tokamak edge), our interest now shifts to the dynamical description of escaping orbits, and the corresponding effect of the internal transport barrier characteristic of a nontwist map.

4. Escape Basins

If we interpret the boundary line $\psi = 1$ as a material wall, any field line hitting this boundary will escape from the system and be lost. The phase portraits depicted in Figs. 2(a)–2(d) are obtained for a Poincaré surface of section, which is the fixed plane $\phi = 0$. The points in the surface of section satisfying the condition $\psi_n \geq 1.0$ can thus be interpreted as field lines escaping through an infinitesimal ring positioned at $\phi = 0$. This is a lowest order approximation of particles escaping through a narrow plate playing the role of a divertor.

Usually, there are more than one divertor plate, chosen so as to collect particles (or field lines) from selected chaotic regions. The detailed design of a divertor is a complicated matter and will not be considered in this work. In order to simplify the physical description we will divide the tokamak wall $\psi = 1$ into two halves: a left (L) exit, for $0 \leq \theta < 0.5$, and a right (R) exit, for $0.5 \leq \theta \leq 1.0$. This procedure transforms our Hamiltonian system into an open one. Once a field line escapes through either of these exits it is considered lost.

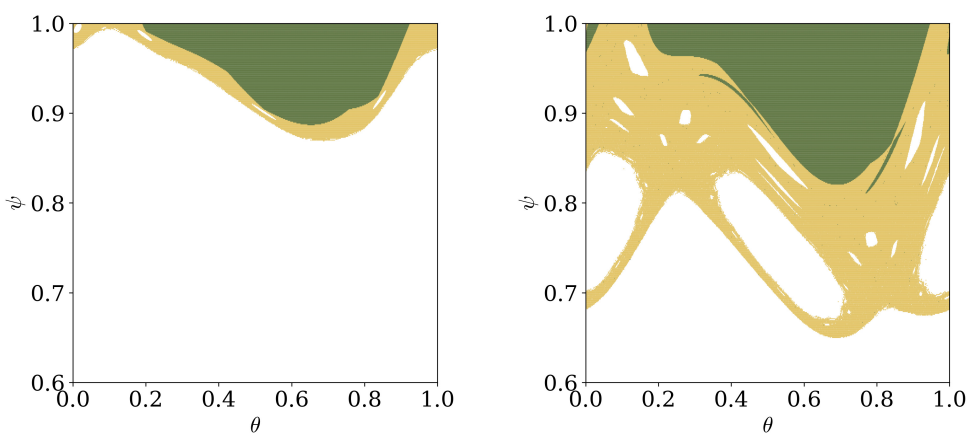

Fig. 4. Escape basins of the Left (green) and Right (yellow) exits at the boundary line $\psi = 1$ for the revtokamap with $K =$ (a) 1.2, (b) 2.0, (c) 2.4 and (d) 6.3. The plots reveal the intricate interplay of escape basins in the $\psi \times \theta$ phase plane, demonstrating increased chaos and mixing within the inner regions as the value of K increases.

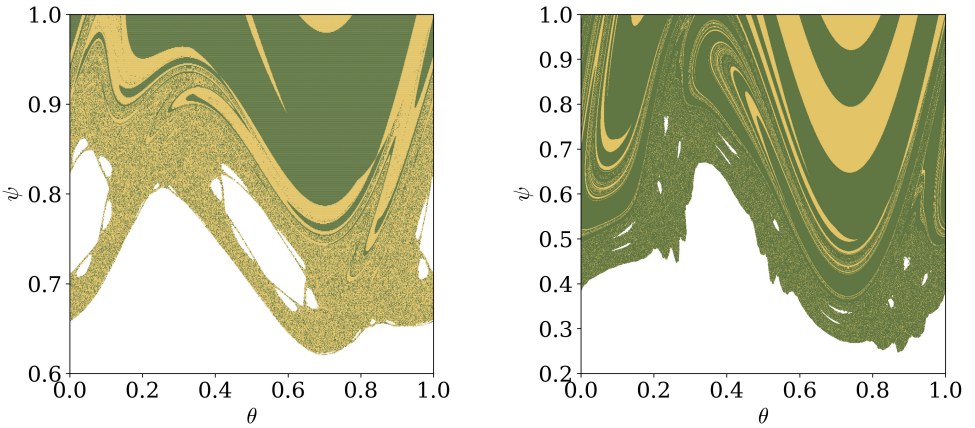

(c) (d)

Fig. 4. (*Continued*)

In this section, we will describe the so-called escape basins, which are the sets of initial conditions, in the $\psi \times \theta$ phase plane, for which the corresponding trajectory (obtained by iterating the revtokamap) escapes through a given exit. Figures 4(a)–4(d) show numerical approximations for the escape basins of the exits L and R, depicted using yellow and green points, respectively. The points left blank are initial conditions for which the trajectories do not escape through any exit. They can be blocked by invariant curves, like those in the plasma core, or either inside periodic islands, also insulated by tori.

The escape basins are more intertwined in the inner tokamak region than being close to the wall itself [Figs. 4(a) and 4(b)]. As the K value increases, the larger area occupied by the chaotic orbit becomes increasingly populated by both escape basins [Figs. 4(c) and 4(d)].

5. Basin Entropy

The escape basins are so densely intertwined in our system that the dimension of the basin escape boundary is practically equal to that of the phase plane. Accordingly, the basin boundary has a structure similar to that of an area-filling curve, like Peano or Hilbert curves. Moreover, the dimension practically does not vary with the parameter K, which is the only available parameter to be varied. Hence the use of the basin boundary dimension does not shed light on the characterization of the fractality of the escape basins, in particular, the degree of final-state sensitivity displayed by them for different values of K.

An alternative approach is to use the novel concept of basin entropy, developed by Daza *et al.* [2016], and which has been extensively used for both dissipative and conservative systems, as a reliable quantification of the fractal structures therein. In the problem we are currently investigating, an open Hamiltonian system, there are two possible outcomes for a chaotic orbit, which are the two exits (L and R) at the tokamak wall $\psi = 1$, corresponding to $\theta < 0.5$ and $\theta > 0.5$, respectively.

We cover the region chiefly occupied by the chaotic region, in the Poincaré surface of section, by a fine mesh of $N \times M$ points. Let us consider the ith rectangular cell belonging to this mesh, and we randomly choose in its interior a large number of initial conditions $(\psi_{i,0}, \theta_{i,0})$. We then determine how many of these initial conditions escape through R (there are n_R of them) or L (n_L). If the trajectory does not escape within a maximum time we discard the initial condition. The corresponding probabilities of escape through L and R are

$$p_L = \frac{n_L}{n_L + n_R}, \quad p_R = \frac{n_R}{n_L + n_R},$$

in such a way that $p_L + p_R = 1$. The information entropy for the ith cell is thus

$$S_i = -p_L \log p_L - p_R \log p_R. \tag{16}$$

Since this entropy is additive (extensive), the total entropy of the mesh will be the sum over all cells, divided by their number

$$S_b = \frac{1}{NM} \sum_{i=1}^{NM} S_i. \tag{17}$$

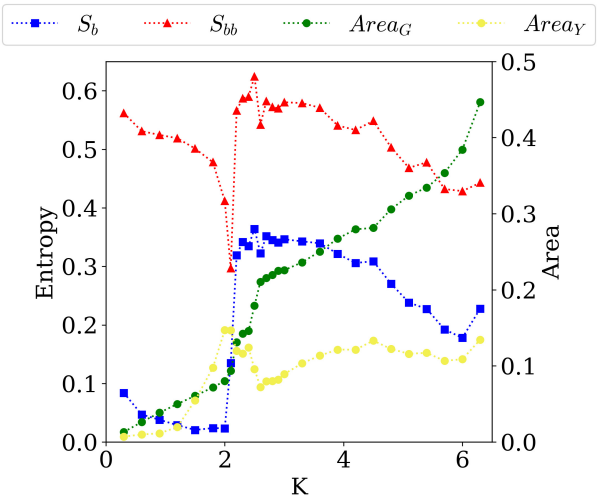

Fig. 5. Basin entropy (blue), basin boundary entropy (red), basin area fraction of green and yellow basins as a function of the parameter K for the revtokamap. The plot shows the relationship between these quantities, revealing an abrupt jump in entropy around $K \approx 2.0$ and a subsequent decrease until $K = 6.0$. These behaviors are closely connected to the distribution of basin areas. Notably, the increasing dominance of the green area leads to a higher probability of finding a single color and consequently results in lower entropy.

Accordingly, the entropy of the escape basin boundary is obtained considering in the sum only those cells that contain points of the boundary between the two escape basins.

The values of the basin entropy for the escape basins of the revtokamap are plotted in Fig. 5 as a function of the parameter K (blue points). It is clearly seen that the entropy, which is nearly zero for $K < 2.0$, suffers an abrupt jump after $K \approx 2.0$ and reaches values between 0.3 and 0.4. In the same figure, we plot the entropy of the escape basin boundary (red points) which are systematically higher than the corresponding values for the basin entropy, which is explained since for S_{bb} we divide the sum in (16) by the number of boxes which actually contains points belonging to the basin boundary. Since the latter is higher than the total number of points, the values of S_{bb} are expected to be always higher than those of S_b. Notice that S_{bb} also experiences a jump near $K = 2.0$, but with less intensity.

For increasing K, the values of basin entropy and basin boundary entropy exhibit a decrease until $K = 6.0$. It is not easy to relate the basin entropy's behavior with the system's dynamics. For comparison, we also plotted in Fig. 5 the fraction of the green and yellow escape basin area as a function of K. The green fraction is shown to increase almost monotonically from low K until $K \approx 6.0$, in contrast, the yellow fraction presents an increase until $K \approx 2$ where it decreases and stays almost constant with an area between 8% and 12%.

6. Wada Property

In systems with fractal basins boundary, a strange phenomena can appear the so-called Wada property, when on boundary point separates simultaneously three or more basins. A point P is a boundary point of a given basin $\mathcal{B}_\in$ if every neighborhood of P is a boundary point of the basin $\mathcal{B}$ and at least another different basin $\mathcal{B}_\in$. If the point P is a boundary point of at least three different basins, then P is a Wada point. If the basin boundary is a fractal curve, and all of its points are Wada then we have a totally Wada fractal curve, if only a fraction of points is Wada, the basin boundary is partially Wada.

As an initial condition is known with a given uncertainty, in a system that exhibits the Wada property, it is impossible to say with precision which exit a particle uses to escape [Kennedy & Yorke, 1991]. The Wada property is an extreme form of final-state sensitivity.

We considered three exits by dividing the tokamak wall $I = 1.0$ into three congruent segments denoted by $L : 0.0 < \psi < 1/3$, $C : 1/3 \leq \psi < 2/3$, and $R : 2/3 \leq \psi \leq 1.0$. Our results are shown in Fig. 6, for $K = 2\pi$. Points belonging to the basins of

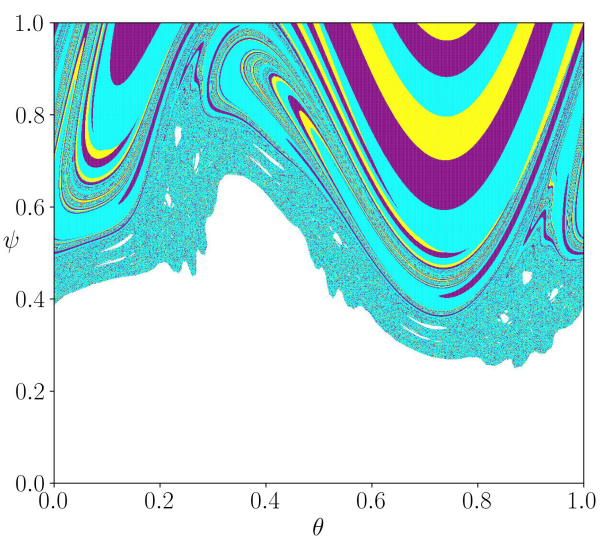

Fig. 6. Basins of escape for the case of three exits with $K = 6.3$. Points belonging to the basins of exits L, C, and R are painted yellow, purple, and aqua, respectively.

L, C, and R are painted yellow, purple, and aqua, respectively.

In order to characterize which boundary points have the Wada property, we used the so-called grid approach [Daza *et al.*, 2015]. Let Ω be a bounded region of the phase space containing $N_A \leq 3$ exits, and let us denote by $\mathcal{B}_j$, $j = 1, 2, \ldots, N_A$, the corresponding basins of escape, we covered Ω by a rectangular grid, with a set of nonoverlapping grid boxes. To each point x of Ω, we assign a function C (color), such that, $C(x) = j$, if x belongs to B_j, if not $C(x) = 0$. We denote by $C(b_j)$ the collection of grid boxes consisting of b_j and all boxes having at least one point in common with b_j. The number of different colors in $C(b_j)$ is $M(b_j)$. Provided $M(b_j) \neq 1, N_A$, we take the two closest boxes in $C(b_j)$ with different colors and draw a line segment between them, calculating the color of the midpoint of this line. If the color of the segment midpoint is such that we have all the possible colors inside $C(b_j)$, then $M(b_j) = N_A$ and we stop the procedure. Otherwise, we choose intermediate points in this line segment and repeat this procedure until $M(b_j) = N_A$, unless the number of points exceeds a specified limit.

We determine the set G_m of those original boxes such that $M(b_j) = m$, for a given integer m. If $m = 1$, we have the set G_1 containing points belonging to the interior of the jth escape basin (interior points). Analogously, the set G_2 contains points belonging to the boundary between two escape basins. Similarly, G_3 consists of points that belong to the boundary

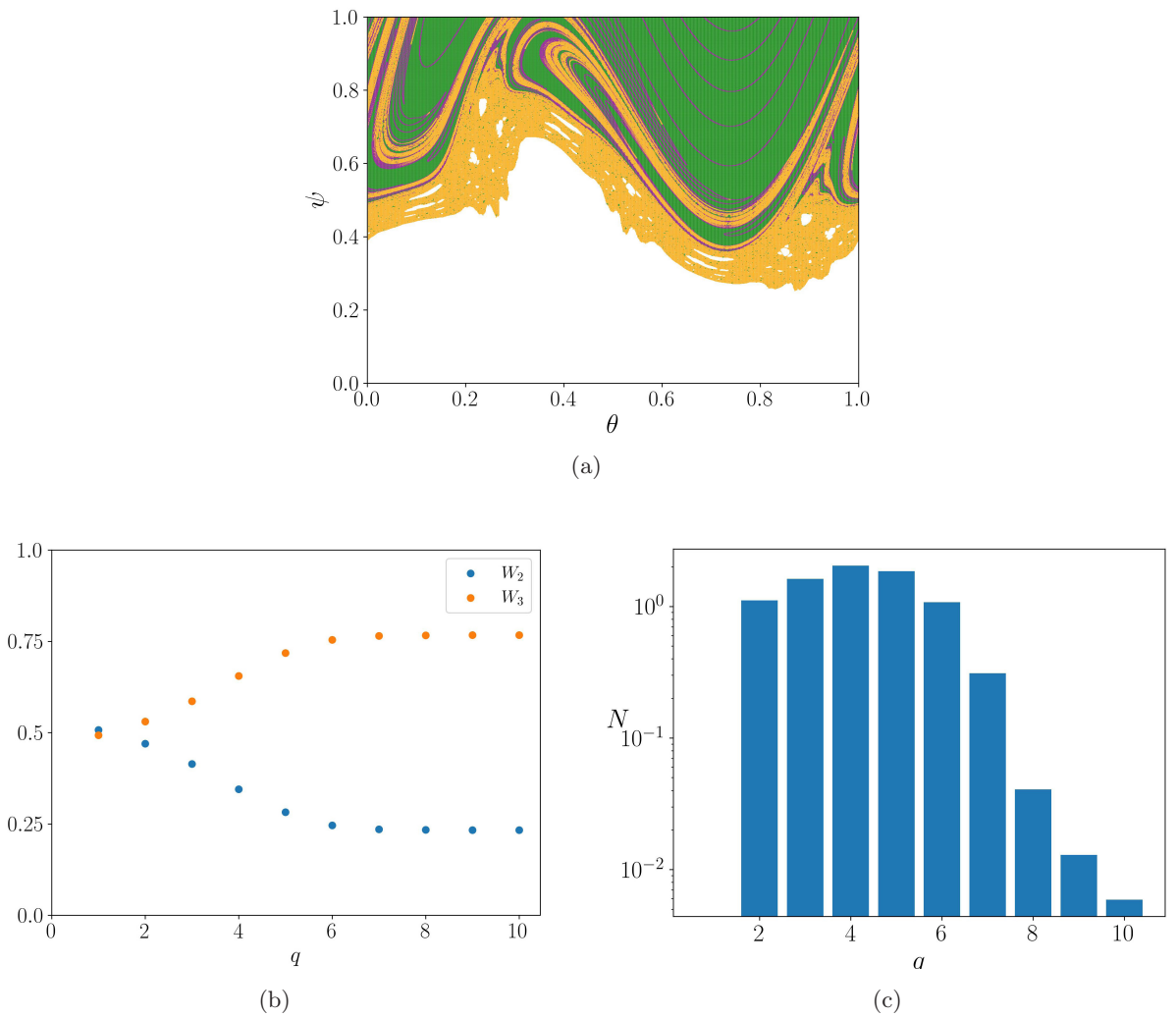

Fig. 7. (a) Basin structure of Fig. 6, showing points belonging to the G_1 set (internal points, green), points of the G_2 set (boundary points between two basins, purple), and points of the G_3 set (boundary points between three basins, orange), after $q = 10$ refinement steps. (b) Values of the quantities W_2 (blue) and W_3 (orange) as a function of the refinement step. (c) Histogram (semilog) showing the number of reclassified points for various numbers of refinement steps.

between three basins, i.e. the set G_3 contains Wada points. Let G_m^q be the set G_m obtained at the qth procedure step. We expect that, as q goes to infinity, the sequence of refinements converge to a final set G_m, in such a way that we compute the following quantity

$$W_m = \lim_{q\to\infty} \frac{\mathcal{N}(G_m^q)}{\sum_{j=2}^{N_A} \mathcal{N}(G_j^q)}, \quad (m = 2, 3, \ldots, N_A), \tag{18}$$

where $\mathcal{N}(G_j^q)$ is the number of points of the set G_j at the qth refinement step. In the case of $W_m = 0$, the system has (almost) no grid boxes that belong to the boundary separating m escape basins. The system is said to have the Wada property if $W_{N_A} = 1$, given that is always possible to find a third color between two other colors. The system is said to be partially Wada when $0 < W_m < 1$, with $m \leq 3$. We considered $N_A = 3$ escape basins, we calculated W_2 and W_3 for an increasing number of q procedure steps, namely

$$W_2 = \frac{\mathcal{N}(G_2)}{\mathcal{N}(G_2) + \mathcal{N}(G_3)}, \tag{19}$$

$$W_3 = \frac{\mathcal{N}(G_3)}{\mathcal{N}(G_2) + \mathcal{N}(G_3)}. \tag{20}$$

For each qth iteration of the procedure, we checked whether or not points of G_2 may belong to G_3 by testing $2(q-2)$ initial conditions which are intermediate between the central box and a neighbor box with a different color. If some of these initial conditions present the missing color, the central box is reclassified as G_3.

Our results, after ten refinement steps, are shown in Fig. 7(a), where we plot the points classified as G_1 (green points), G_2 (purple points) and G_3 (orange points). We observe a predominance of Wada points belonging to the set G_3, in agreement with the complex basin structure displayed by Fig. 6. Moreover, the values of W_2 and W_3 are shown in Fig. 7(b) as a function of q. We observe a fast convergence after just $q = 6$ iterations, yielding $W_2 \approx 0.233$ and $W_3 \approx 0.767$. Hence the basins of escape are partially Wada. The fast convergence can also be seen in Fig. 7(c), which shows a histogram for the number of points initially classified as belonging to the set G_2 but which are reclassified to the G_3 set in each refinement step, after a large number of evaluations of the quantities W_2 and W_3. We see that most of the convergence is obtained after 3 to 7 steps, and the number of reclassified points decreases exponentially to zero as q increases.

7. Conclusions

The particles inside a fusion reactor can have a complex trajectory and behavior and its description can turn out to be a very complicated system of equations by trying to include all the complex phenomena present in a tokamak. Simplifying the description can reveal some exciting properties and behaviors hidden by the large quantities of parameters and conditions. The *RevTokamap* introduced by Balescu is an outstanding example of a model of the field lines with the property of reversed shear and a great physical sample of a nontwist map.

Being a nontwist map, it shares some fundamental properties with the standard nontwist map that has been largely studied. One of the most important properties shared by both is the presence of a transport barrier, that produces a division between two regions on the map. In the revtokamap there is the division between the particles in the plasma core and the particles that escape to the walls, the presence of that transport barrier can improve the quality of confinement by preventing the exchange of particles in the two regions, and preventing the particles in the plasma core to escape.

The presence of escape basins, or basins of attraction, is another common property in nontwist maps. The continuity of a basin boundary can infer the uncertainty of the initial condition of a given physical system and we can relate this to the basin's entropy of a given system.

The basin entropy measure allows us to quantify the level of uncertainty and predictability within the escape basins of the system. By examining the variation of basin entropy with the parameter K, we observe an intriguing abrupt jump and subsequent decrease, indicating a significant change in the dynamics of the system. This observation suggests the presence of critical transitions and the emergence of new dynamical behaviors as K surpasses a certain threshold near $K = 2.0$ where the basins are sharply divided having a continuous line that separates the basins, this provides the lowest mixture, and therefore the lowest value of entropy.

Raising the value of K near the critical point, the basins start to mix and the green basin grows continuously until it occupies almost half of the phase space when $K = 2\pi$. The growing expansion

of the green basin leads to less uncertainty in the initial conditions, due to the existence of the transport barrier, there is a limited value of initial conditions that can escape, so there is a loss of entropy with the dominance of one escape basin.

The addition of the shearless curve in the revtokamap brings a greater knowledge about how the perturbation parameter influences and how the particles escape through the walls of a tokamak but using a relatively simple map. Being a nontwist map also allows exploring some interesting properties like the transport barrier that limits the occupied area by the escape basins and influences the entropy. The preference for the particles to escape through the right exit is even more noticeable when the escape line is divided into three and we see a predominance toward that exit. This also reveals the presence of the Wada property, showing that uncertainty in the escape basin remains.

We employ the Wada property as a complementary measure to assess the mixing characteristics of the *RevTokamap*. The Wada property provides valuable information about the extent to which trajectories originating from different regions mix within the phase space. By studying the Wada property in conjunction with basin entropy, we can elucidate the role of chaos and mixing in the transport of field lines and particles within the tokamak.

Acknowledgments

This work has been supported by grants from the Brazilian Government Agencies CNPq(proc. 140920/2022-6, 140713/2020-4, 403120/2021-7, and 301019/2019-3) CAPES(proc. 88881.143103/2017-01) and FAPESP(grant. 2022/04251-7 and 18/03211-6).

References

Aguirre, J., Viana, R. L. & Sanjuán, M. A. [2009] "Fractal structures in nonlinear dynamics," *Rev. Mod. Phys.* **81**, 333.

Balescu, R. [1988] *Transport Processes in Plasmas* (North-Holland).

Balescu, R. [1998] "Hamiltonian nontwist map for magnetic field lines with locally reversed shear in toroidal geometry," *Phys. Rev. E* **58**, 3781.

Balescu, R., Vlad, M. & Spineanu, F. [1998] "Tokamap: A Hamiltonian twist map for magnetic field lines in a toroidal geometry," *Phys. Rev. E* **58**, 951.

Bittencourt, J. A. [2004] *Fundamentals of Plasma Physics* (Springer Science & Business Media).

Daza, A., Wagemakers, A., Sanjuán, M. A. & Yorke, J. A. [2015] "Testing for basins of Wada," *Scient. Rep.* **5**, 16579.

Daza, A., Wagemakers, A., Georgeot, B., Guéry-Odelin, D. & Sanjuán, M. A. F. [2016] "Basin entropy: A new tool to analyze uncertainty in dynamical systems," *Scient. Rep.* **6**, 31416.

del Castillo-Negrete, D. & Morrison, P. [1993] "Chaotic transport by rossby waves in shear flow," *Phys. Fluids A*: *Fluid Dyn.* **5**, 948–965.

Hazeltine, R. D. & Meiss, J. D. [2003] *Plasma Confinement* (Courier Corporation).

Kennedy, J. & Yorke, J. A. [1991] "Basins of Wada," *Physica D* **51**, 213–225.

Lichtenberg, A. J. & Lieberman, M. A. [2013] *Regular and Chaotic Dynamics*, Vol. 38 (Springer Science & Business Media).

Mathias, A., Kroetz, T., Caldas, I. & Viana, R. [2017] "Chaotic magnetic field lines and fractal structures in a tokamak with magnetic limiter," *Chaos Solit. Fract.* **104**, 588–598.

Mathias, A., Perotto, G., Viana, R., Schelin, A. & Caldas, I. L. [2022] "Fractal structures and magnetic footprints in a divertor tokamak," *Int. J. Bifurcation and Chaos* **32**, 2250078-1–14.

Ott, E. [2002] *Chaos in Dynamical Systems* (Cambridge University Press).

Szezech Jr, J., Caldas, I. L., Lopes, S. R., Morrison, P. & Viana, R. L. [2012] "Effective transport barriers in nontwist systems," *Phys. Rev. E* **86**, 036206.

Viana, R., Caldas, I. L., Szezech Jr, J., Batista, A., Abud, C., Schelin, A., Mugnaine, M., Santos, M., Leal, B., Bartoloni, B. *et al.* [2021] "Transport barriers in symplectic maps," *Brazilian J. Phys.* **51**, 899–909.

Wiggins, S. [2013] *Chaotic Transport in Dynamical Systems*, Vol. 2 (Springer Science & Business Media).

Wolf, R. [2002] "Internal transport barriers in tokamak plasmas," *Plasma Phys. Contr. Fusi.* **45**, R1.